Physica D 280–281 (2014) 48–58

Contents lists available at ScienceDirect

Physica D

journal homepage: www.elsevier.com/locate/physd

Quantification and prediction of extreme events in a one-dimensional nonlinear dispersive wave model

Will Cousins, Themistoklis P. Sapsis *

Department of Mechanical Engineering, Massachusetts Institute of Technology, 77 Massachusetts Av., Cambridge, MA 02139, United States

HIGHLIGHTS

- Probabilistic analysis of extreme events in a nonlinear dispersive wave model.
- Analytical characterization trigger condition for extreme events.
- Characterization of the energy transfers through a Gabor basis, localized approach.
- Formulation of a predictive scheme for extreme events.

ARTICLE INFO

Article history:
Received 14 January 2014
Received in revised form
17 April 2014
Accepted 30 April 2014
Available online 10 May 2014
Communicated by T. Wanner

Keywords:
Prediction of extreme events
Rogue waves
Dispersive nonlinear waves
Intermittent instabilities
Nonlinear energy transfers
Probabilistic quantification of rare events

ABSTRACT

The aim of this work is the quantification and prediction of rare events characterized by extreme intensity in nonlinear waves with broad spectra. We consider a one-dimensional nonlinear model with deep-water waves dispersion relation, the Majda–McLaughlin–Tabak (MMT) model, in a dynamical regime that is characterized by a broadband spectrum and strong nonlinear energy transfers during the development of intermittent events with finite-lifetime. To understand the energy transfers that occur during the development of an extreme event we perform a spatially localized analysis of the energy distribution along different wavenumbers by means of the Gabor transform. A statistical analysis of the Gabor coefficients reveals (i) the low-dimensionality of the intermittent structures, (ii) the interplay between non-Gaussian statistical properties and nonlinear energy transfers between modes, as well as (iii) the critical scales (or critical Gabor coefficients) where a critical amount of energy can trigger the formation of an extreme event. We analyze the unstable character of these special localized modes directly through the system equation and show that these intermittent events are due to the interplay of the system nonlinearity, the wave dispersion, and the wave dissipation which mimics wave breaking. These localized instabilities are triggered by random localizations of energy in space, created by the dispersive propagation of low-amplitude waves with random phase. Based on these properties, we design low-dimensional functionals of these Gabor coefficients that allow for the prediction of the extreme event well before the nonlinear interactions begin to occur.

1. Introduction

Extreme or rare events have attracted substantial attention in various scientific fields both because of their catastrophic impact but also because of the serious lack of specialized mathematical tools for the analysis of the underlying physics. Important examples can be found in (i) the environmental field: rogue waves in the ocean [1–4], extreme weather and climate events [5,6], and (ii) the engineering field: overloads and failures in power grids [7,8], stability loss and capsizing of ships in mild waves [9]. For all of the above applications it has now been well established that extreme events occur much more frequently than it was initially believed and that their traditional characterization as 'rare events' (especially in a Gaussian context where a rare event has practically zero probability) severely underestimates the frequency of their occurrence. Therefore, it is important to study them more thoroughly and develop effective algorithms for their prediction.

Extreme events refer to system responses with magnitude that is much larger than the typical deviation that characterizes the system response. Of particular interest are extreme events that occur far more likely than Gaussian statistics would suggest. Interest in such heavy-tailed behavior is not merely academic, as heavy-tailed statistics have been observed both numerically [10] and experimentally [11] in the context of directional water waves. In such

* Corresponding author. Tel.: +1 617 324 7508; fax: +1 617 253 8689.
E-mail addresses: sapsis@mit.edu, themis.sapsis@gmail.com (T.P. Sapsis).

http://dx.doi.org/10.1016/j.physd.2014.04.012
0167-2789/

cases it can be concluded that traditional analysis tools restricted to second order statistics would not be sufficient for their understanding. Apart from their intermittent properties, another manifestation of the non-Gaussian character of extreme events is the strong localization of energy in (physical or modal) space—a situation that is inherently connected with non-linear dynamics and transient or persistent instabilities, which has been shown (see e.g. [12,13]) to be an important factor that can lead to non-Gaussian statistics.

These characteristics also define the modeling challenges for the study of these systems, with the most important being the interplay of a few intermittent modes with a large number of modes that act as a 'reservoir' of energy for the former. In the case considered in this work (the MMT equation), this large set of modes is usually characterized by a broadband spectrum consisting of dispersive waves with weakly non-Gaussian statistics that propagate and sporadically give rise to extreme, localized events. In contrast to this large set of waves, extreme events are characterized by strong nonlinear energy transfers and non-Gaussian statistics. Therefore, we have on the one hand a nearly Gaussian 'heat bath' of waves that propagate in the presence of dispersion which leads to energy localization in random scales and places, and on the other hand a nonlinear mechanism that uses the former as excitation to generate extreme events [14].

It is clear from the above discussion that a mathematical framework able to handle problems characterized by extreme events should include higher order statistics and also should be able to deal with the inherent nonlinear character of the underlying dynamics. However, the computational cost associated with these requirements would be enormous since (i) the number of physical degrees of freedom is usually very large and (ii) because the description of non-Gaussian properties and in particular the description of rare events that 'live' in the tails of the distribution requires a substantial amount of realizations which is very hard to obtain and process in a direct Monte-Carlo framework. In addition, a purely statistical understanding cannot provide a rigorous analysis of the underlying physical mechanisms.

On the other hand, order-reduction approaches based, for example, on Polynomial Chaos expansions or Proper Orthogonal decompositions have proven to be of limited applicability in nonlinear systems with intermittency [15]. Due to their localized spatial and temporal characters, extreme events carry only small amounts of energy compared with other global modes that characterize the full response field. Therefore, standard order-reduction techniques will most likely miss the essential parts of the extreme event dynamics.

To simulate the dynamical mechanisms that lead to the generation of extreme events, we use the MMT model, a one-dimensional nonlinear dispersive equation originally proposed by Majda, McLaughlin, and Tabak to assess the validity of weak turbulence theory [16]. MMT admits four-wave resonant interactions and, when coupled with large-scale forcing and small-scale damping, admits a rich family of spectra exhibiting direct and inverse cascades [17,18]. Zakharov et al. have also analyzed the MMT model in detail and have used large amplitude coherent structures present in MMT as models of extreme ocean waves [19–21]. In this work, we analyze in detail the 'solitonic' coherent structures in the focusing MMT, which have also been investigated by Cai et al. [18]. In their early stages, these localized structures resemble self-similar spatial collapses and rapidly transfer energy to small scales where it is dissipated [18]. We are particularly interested in these localized structures as they generate states which are extreme compared to the benign background out of which they arise.

In the present work, we first aim to develop analytical and numerical tools in order to understand how these localized extreme events are triggered by spatially localized perturbations in the MMT model. We illustrate that there is a critical spatial lengthscale and a critical amount of energy associated with it that leads to the occurrence of extreme solutions. This critical scale is the result of the interplay between wave dispersion, wave nonlinearity and selective dissipation that occurs in high wavenumbers. For perturbations of a zero background state we are able to analyze this phenomenon directly by deriving a family of scale invariant solutions. However, the critical amount of energy depends also on the background energy level of the system, the effects of which we analyze numerically. In contrast to the standard linearized analysis, which considers small Fourier mode perturbations about a given state, the framework presented here considers spatially localized perturbations that are not necessarily small.

We illustrate that these extreme events are characterized by low-dimensionality and we use a spatially localized basis, a Gabor basis, with localization characteristics tuned according to the results of the previous conclusions. Using the projected information of the extreme events to this localized basis we perform a statistical analysis of the Gabor coefficients to reveal the strongly non-Gaussian character associated with the strongly nonlinear interactions of these modes during an extreme event. Note that this statistical structure, which is directly connected to the nonlinear energy transfers that take place, is otherwise 'buried' in the broadband spectrum of the full wave field and its only signature in the stochastic field response is the heavy tail statistics.

Finally, we formulate predictive functionals that efficiently characterize the domain of attraction to the extreme event solutions. These predictive functionals are formulated in a probabilistic fashion in terms of the Gabor coefficients that correspond to the critical lengthscales. Given the current information of the wavefield, they provide the probability of occurrence of an extreme event in a later time instant. Note that the propagation of waves (having random phases) in the presence of dispersion creates conditions for localization of energy in arbitrary scales and positions in space. The formulated probabilistic functionals assess these random localizations of energy and quantify the probability that they will lead to an occurrence of an extreme event in the future.

2. A one-dimensional, dispersive nonlinear prototype model with intermittent events

We consider the following one-dimensional partial differential equation originally proposed by Majda, McLaughlin, and Tabak [16] for the study of 1D wave turbulence:

$$iu_t = |\partial_x|^{\alpha} u + \lambda |\partial_x|^{-\beta/4} \left(\left| |\partial_x|^{-\beta/4} u \right|^2 |\partial_x|^{-\beta/4} u \right) + iDu \qquad (1)$$

where u is a complex scalar. On the real line, the pseudodifferential operator $|\partial_x|^{\alpha}$ is defined through the Fourier transform as follows:

$$\widehat{|\partial_x|^{\alpha} u}(k) = |k|^{\alpha} \widehat{u}(k).$$

This operator may also be defined analogously on a periodic domain. The MMT equation was introduced on the basis of a simple enough model to test thoroughly the predictions of weak turbulence theory. In the context of dispersive nonlinear waves it provides a prototype system with non-trivial energy transfers between modes or scales, non-Gaussian statistics with heavy tails, and intermittent events with high intensity, while remaining accessible to high resolution simulations [16–18,22]. Therefore, it is an ideal basis to assess the performance of probabilistic quantification algorithms for the occurrence and prediction of extreme events.

In the present work the parameter α is set to $1/2$ as this matches the dispersion relation for deep water waves $\omega^2 = |k|$. Setting $\alpha = 2$ and $\beta = 0$ in (1) yields the nonlinear Schrödinger equation (ignoring the dissipation term). As in [16] we include dissipation at small scales (modeling e.g. wave breaking in the context of

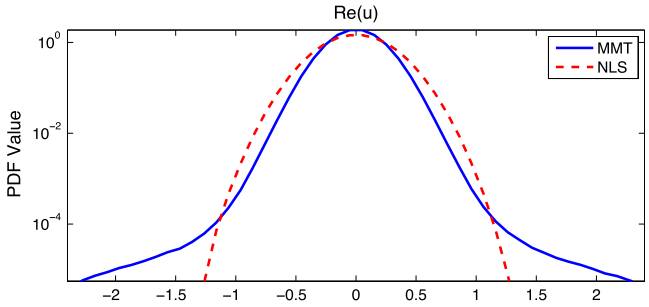

Fig. 1. Probability density for the real part of u for simulations of NLS and MMT ($\alpha = 1/2$, $\beta = 0$).

water waves) through a selective Laplacian operator Du, defined in Fourier space:

$$\widehat{Du}(k) = \begin{cases} -(|k| - k^*)^2 \hat{u}(k) & |k| > k^* \\ 0 & |k| \le k^*. \end{cases}$$

Similar dissipation models have been used in more realistic settings involving ocean water waves [23]. The critical wavenumber is taken as $k^* = 500$ which is a value that is large enough so that it allows for the development of nonlinear instabilities that lead to extreme waves and small enough to create energy cascades in higher wavenumbers and thus, allow for these waves to exist only for finite time.

For the nonlinearity coefficient we choose $\lambda = -4$. Our goal here is to study a prototype system that generates rare events of extreme intensity. With this in mind, we use $\lambda < 0$, corresponding to the focusing case, which gives rise to intermittent extreme events generated by collapsing solitons [17,18]. We choose $\lambda = -4$ since, with the chosen initial data (see the next paragraph), this value corresponds to 3–4 extreme events per 100 time units (100 time units being a moderately long time length relative to the time scales in the considered MMT simulations). This choice is not based on physical principles—the chosen extreme event frequency is a happy medium where such events occur often enough to be characterized statistically by Monte Carlo simulation but sparsely enough to be considered rare. Although we chose to vary λ to control the extreme event frequency, an identical effect could have been obtained by fixing $\lambda = -1$ and merely rescaling $u(x, 0)$.

We consider the evolution of a sum of Fourier modes with independent, uniformly distributed random phases, meaning that initially u has a nearly Gaussian distribution. For a linear model, the distribution would remain nearly Gaussian as the modes evolve independently. Interestingly, even in simulations of the focusing nonlinear Schrödinger equation (NLS) we find that u remains nearly Gaussian. However, for the MMT model we find that the distribution u develops heavy tails with an exponential decay rate (see Fig. 1). We stress that although for the simulations considered here the NLS simulations generate Gaussian statistics, this is not always the case. Heavy-tailed statistics have been observed by other authors in numerical simulations of the focusing NLS equation [24,10].

The heavy tails in solutions of MMT are induced by the intermittent formation and subsequent collapse of localized extreme events arising out of a nearly Gaussian background. Fig. 2 displays the origination and disappearance of such an extreme event. In their early stages these extreme events resemble the collapses that are present in focusing MMT with no dissipation. In these collapses, which have been described by Cai et al. [18], energy is dramatically transferred to smaller scales and the solution experiences a singularity in finite time. In our simulations, the small-scale dissipation included in (1) (modeling wave breaking in the context of water waves) ensures that u remains regular for all times. Collapse dynamics have been found to induce heavy-tailed statistics in other situations as well, such as the damped-driven quintic 1D nonlinear Schrödinger equation [25].

2.1. Numerical simulation and computation of statistics

We solve (1) for $x \in [0, 2\pi]$ with periodic boundary conditions using a Fourier method in space combined with a 4th order Runge–Kutta exponential time differencing scheme [26,22]. This scheme requires evaluation of the function $\phi(z) = (e^z - 1)/z$. Naive computation of ϕ can suffer from a numerical cancellation error for small z [27]. We use a Padé approximation code from the EXPINT software package, which does not suffer from such errors [28]. We use 2^{13} Fourier modes with a time step of 10^{-3}; results in this work were insensitive to further refinement in grid size.

For the statistical studies performed in this work, we evolve a sum of 31 Fourier modes with independent, uniformly distributed random phases. We compute statistics by averaging over time and space over 300 ensembles, each spanning 100 time units ($t = 100$ to $t = 200$). There is no external forcing in our simulations and all the energy of the system comes through the initial conditions while dissipation occurs whenever an extreme event takes place. To this end, we do not observe an exact statistical steady state in our simulations, but after an initial transient where a moderate amount of energy is dissipated through selective damping, the solution settles to a nearly (or very slowly varying) statistical steady state where the L^2 norm decays slowly (see Fig. 3). We focus on this slowly varying regime where roughly 2–4 extreme events occur per simulation in the time window $t \in [100, 200]$, and, as shown in Fig. 3, these extreme events are uniformly prevalent (roughly) throughout this time window (although they are slightly more common for earlier times). In Fig. 3, extreme events are identified as local maxima of $|u|$ that exceed 2.5. This threshold value of 2.5 corresponds to 8 typical deviations of the wave field, consistent with the information definition of rogue waves in the ocean [1].

3. Nonlinear instabilities induced by spatially localized energy

In this section we examine the role of *spatially localized* energy in the formation of an extreme event. More specifically, we define the energy E of a solution as

$$E \triangleq r^2 = \int \left|u^2(x)\right| dx,$$

where r is the L^2 norm of the solution, which is conserved by undamped MMT [19]. In the undamped MMT equation, localized initial data with energy above some critical level leads to a finite time blowup [18,19]. Here we examine how this critical energy level varies with the degree of initial energy localization, as well as the energy of the background state, in the presence of selective dissipation. Both of these parameters are important to determine the critical scale that is most sensitive for the formation of an extreme event. For the zero background case, we are able to analytically determine this relationship by deriving a scale invariant family of solutions. We investigate the non-zero background case numerically.

Zero background energy: scale invariant solutions. We begin our analysis by focusing on localized perturbations when we have zero energy background in the system. More specifically, we consider a family of initial data of the form $u(x, 0) = u_0(x; c, L) = ce^{-2(x/L)^2}$ and determine how the critical energy level required for blow-up depends on the lengthscale L. To do so, we derive an L-parametric family of solutions w_L, $L > 0$, defined by the scaling of a given solution $u(x, t)$

$$w_L(x, t) = \frac{1}{L^p} u\left(\frac{x}{L}, \frac{t}{L^q}\right).$$

To determine p and q, we plug this ansatz into MMT with no dissipation, which gives:

$$\frac{i}{L^{p+q}} u_t = \frac{1}{L^{p+\alpha}} |\partial_x|^\alpha u + \frac{\lambda}{L^{3p-\beta}} |\partial_x|^{-\beta/4} \left(\left| |\partial_x|^{-\beta/4} u \right|^2 |\partial_x|^{-\beta/4} u \right).$$

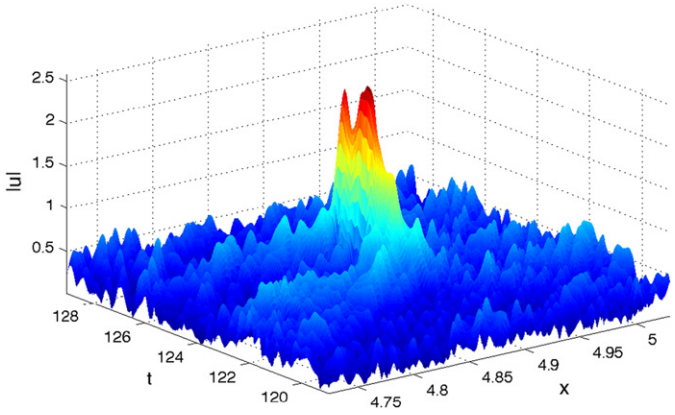

Fig. 2. Example of an extreme event arising out of a weakly non-Gaussian 'heat bath' of dispersive waves with random phase.

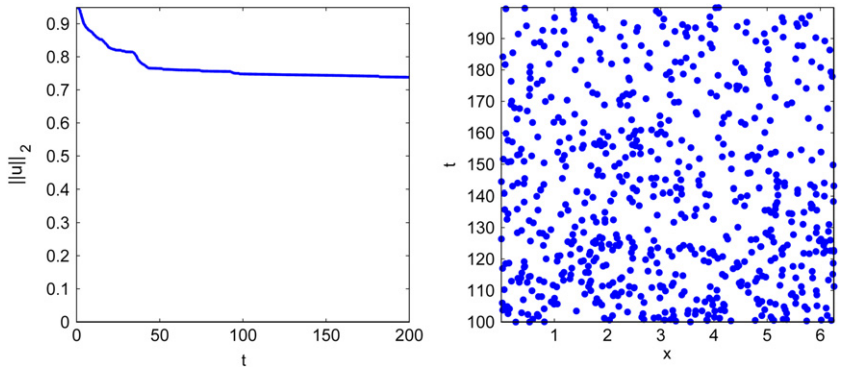

Fig. 3. Left: decay of L^2 norm of the solution; after 100 time units the decay rate becomes small. Right: locations of extreme events in an ensemble of simulations.

So w is also a solution to MMT if $q = \alpha$ and $p = (\alpha + \beta)/2$, giving us the following family of solutions:

$$w_L(x, t) = \frac{1}{L^{(\alpha+\beta)/2}} u\left(\frac{x}{L}, \frac{t}{L^\alpha}\right).$$

Therefore, if for a reference lengthscale $L = 1$, we have the critical energy norm $r_{\text{crit}}(1)$ (associated with an initial condition $u_0(x; c^*, 1)$) that leads to a blow-up solution, the corresponding critical energy for initial data localized for an arbitrary lengthscale L will be

$$r^2_{\text{crit}}(L) = \frac{1}{L^{\alpha+\beta}} \int u_0^2\left(\frac{x}{L}; c^*, 1\right) dx = L^{1-\alpha-\beta} r^2_{\text{crit}}(1).$$

Hence, the critical energy norm $r_{\text{crit}}(L)$ required to initiate a blow-up is given by

$$r_{\text{crit}}(L) = L^{(1-\alpha-\beta)/2} r_{\text{crit}}(1). \tag{2}$$

We consider the special case $\alpha = 1/2$, $\beta = 0$, which gives

$$r_{\text{crit}}(L) = \sqrt[4]{L} r_{\text{crit}}(1). \tag{3}$$

Since the above function decreases to 0 as L becomes small, in the deep water wave dispersion case only a *small amount of localized energy* is sufficient to initiate a blow-up. This fact holds as long as the exponent of L in (2) is positive, meaning $\beta < 1 - \alpha$, or simply $\beta < 1/2$ using the standard value of $\alpha = 1/2$. Pushkarev and Zakharov [21] use $\beta = -3$ to study extreme waves, which is small enough to ensure that this relationship between localization and energy criticality still holds. In fact, with $\beta = -3$ we have $r_{\text{crit}}(L) = L^{7/2} r_{\text{crit}}(1)$, so this relationship ($r_{\text{crit}}$ decreasing as L decreases) would presumably be even stronger than the $\beta = 0$ case we consider.

Note that for the case that selective dissipation is present, very localized amounts of energy will be rapidly dissipated. In particular, if energy is *too* localized, then the selective Laplacian damping is dominant compared with the instability of the nonlinear terms and the amplitude of u decreases relative to its initial state. However, for values of L that are not excessively small, we have a rapid growth of the amplitude of u that leads to an energy cascade (see the next section) to smaller scales and subsequent dissipation by the selective Laplacian. In this way the high wavenumber damping prevents the formation of a singularity due to continuous energy transfer and accumulation to infinitesimally small scales and results in a finite lifetime for the extreme event (Fig. 2). This behavior has been noted previously for MMT with forcing and dissipation by Grooms and Majda [22].

Therefore, in the damped MMT, for each localization scale L that is not excessively small we expect there to be a critical amount of energy that will trigger a nonlinear instability resulting in an extreme event. We expect that, except for excessively small values of L, the above analysis will still hold and the dissipation will only become relevant in the late stages of an extreme event where it prevents the formation of a singularity. We quantify the critical energy for the damped system using two different measures. First, we compute the finite-time divergence of nearby (in terms of energy) initial perturbations through the quantity

$$|\partial_r q(r, L)| \triangleq \left| \frac{\partial}{\partial r} \frac{\max_{x,t} |u(x, t; r)|}{\max_x u(x, 0; r)} \right|.$$

This quantity is displayed by a color plot in Fig. 4. We use the sharp ridge of $|\partial_r q|$ to determine the critical energy level at which the transition to extreme events occurs. Additionally, we determine the critical energy level by determining the set of values (r, L) at which $q(r, L) > 1.5$. The black curve in Fig. 4 outlines the region where q exceeds this threshold value. This curve compares favorably with the results from the first method. Also in Fig. 4 we present

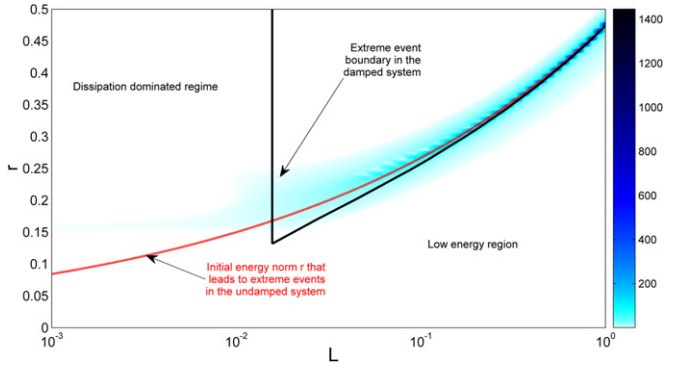

Fig. 4. Critical energy norm of a localized perturbation that leads to the formation of an extreme event for the undamped (red dashed curve) and the damped MMT model in the absence of background energy. The latter is described in terms of the finite-time divergence q of nearby trajectories (color map) and the maximum value of the response field $|u|$. (For interpretation of the references to color in this figure legend, the reader is referred to the web version of this article.)

with a red dashed curve the critical energy norm for the undamped system, given by (3). We emphasize that even though Fig. 4 was generated by numerically solving (1) on a domain of size 16π with periodic boundary conditions, these results do not change if the domain size is increased further due to the localization of these examples. This behavior contrasts sharply with similar experiments of the nonlinear Schrödinger equation, where the values of $|q|$ never become large and the sharp gradient seen in Fig. 4 does not occur.

We note that for the case of the damped system the critical energy norm closely resembles the analytical prediction (3), which is a result of the interplay between dispersion and nonlinearity. This is the case until we reach the critical scale L_c, below which dissipation is important and no extreme solutions can occur. To this end this spatial scale L_c is the most sensitive to localized perturbations i.e. it can be triggered with the lowest amount of energy, and it is essentially the smallest scale where dissipation is still negligible. The existence of this critical scale that triggers extreme events is the result of the synergistic action of dispersion, nonlinearity, and small-scale dissipation.

Case of finite background energy. We now consider the formation of an extreme event out of a background with non-zero energy, that is, we evolve initial data of the form $u(x, 0) = b + ce^{-2(x/L)^2}$. We first consider the case of small ratio $\frac{c}{b} \ll 1$ where we can investigate the evolution of u by performing a linearized stability analysis about the following exact, spatially constant solution of MMT with arbitrary α and $\beta = 0$, $u(x, t) = be^{-i\lambda b^2 t}$.

For the nonlinear Schrödinger equation with periodic boundary conditions, this solution is unstable to Fourier mode perturbations of wavenumber n when the following condition is satisfied:

$$n < \frac{L_x}{2\pi}\sqrt{-2\lambda b^2},$$

where L_x is the domain width. The above is known as the Benjamin–Feir instability and has been studied extensively by many authors [29–32].

In the context of the undamped MMT equation, the Benjamin–Feir instability can be generalized. In particular one can show that for the case $\beta = 0$, the spatially constant solution is unstable if $\lambda < 0$ and

$$n < \frac{L_x}{2\pi}\left(-2\lambda b^2\right)^{1/\alpha}. \tag{4}$$

Clearly, for $\alpha = 2$, the above result agrees exactly with the classical Benjamin–Feir instability criterion of NLS. For NLS, u is the envelope of a slowly modulated carrier wave, so the spatially constant solution studied here corresponds to a plane wave solution for the surface elevation oscillating at the carrier frequency. For MMT with $\alpha = 1/2$, there is a more complicated relationship between u and the associated surface elevation [21], but a spatially constant u corresponds to a spatially constant surface elevation. Here we have only analyzed the linearized stability of a single periodic solution to MMT (specifically, the 0-mode solution). For the purposes of our analysis this is sufficient, but MMT admits a family of periodic solutions whose linear stability has been documented in detail by Rumpf and Newell [33].

We emphasize that although the Benjamin–Feir modulation instability is present in both the focusing MMT and the NLS, its manifestation is not the same in each case. We illustrate this fact by numerical experiments involving no selective damping. For both equations, we take $\lambda = -4$ and $L_x = 2\pi$, meaning that the critical value of b in (4) is roughly 0.35. Values of b larger than this admit at least one unstable mode, and positive b less than this value have no unstable modes. We evolve initial data of the form $u(x, 0) = b + \epsilon\cos(x)$ with $b \approx 0.34$ and $b \approx 0.36$. For each value of b, we set $\epsilon = 0.01$. When $b \approx 0.34$, the small perturbation does not grow for the MMT or the NLS, agreeing with the linearized analysis (see Fig. 5). For the NLS, unstable perturbations of this kind initiate a nearly-periodic orbit where large, but bounded, coherent structures repeatedly appear and subsequently dissolve in a Fermi–Pasta–Ulam-like recurrent cycle [34,32]. However, in the MMT, these unstable perturbations grow continuously and collapse into a singularity in finite time (see Fig. 5). This mechanism of collapse initiation via modulation instability, which has also been studied by Cai et al. [18], has significant implications for our critical energy analysis for the nonzero background case. Although including high frequency damping will prevent the formation of a singularity, such damping will not prevent an extreme event from occurring since it only becomes relevant after energy has been transferred to the small scales; that is, after an extreme event has already occurred (as in Fig. 2). Thus, if b and L_x satisfy the Benjamin–Feir instability criterion (4) with $n = 1$, initial conditions of the form $u(x, 0) = b + ce^{-2(x/L)^2}$ will initiate an extreme event for any $c > 0$.

Fig. 6 displays the critical energy norm of the perturbation $ce^{-2(x/L)^2}$ required to initiate an extreme event for various values of b and L. For $b = 0$, this critical amplitude is precisely the curve described above and displayed in Fig. 4, and for large enough b this critical amplitude is infinitesimal due to the Benjamin–Feir instability. For intermediate values of b, the critical amplitude presents a smooth transition between the two theoretically understood regimes. For $b = 0$, we noted previously that the more localized the energy is, the smaller the amount of this energy is required to initiate a blowup. This fact remains true for nonzero background energy b until the point where b is large enough so that a Benjamin–Feir instability occurs, which in this case ($L_x = 8\pi$, $\lambda = -4$, $\alpha = 1/2$) occurs at $b = 0.25$. The surface displayed in Fig. 6 is another example showing that local, non-infinitesimal perturbations can initiate extreme responses with background levels below the Benjamin–Feir energy threshold as a result of the interplay between nonlinearity, dispersion and dissipation.

4. Statistics of nonlinear dynamics during an extreme event

So far we have examined the conditions that lead to extreme wave solutions. In this section we will study the nonlinear interactions taking place during the occurrence of an extreme event by statistical analysis after projecting the solution u onto an appropriate localized set of modes. Given the localized character of extreme events, global basis elements such as Fourier modes will not be able to describe effectively their dynamical properties since, despite their large amplitude, extreme events carry very small portion of energy of the overall field spectrum.

To this end, it is more informative to choose a set of modes which incorporate the localized character of the extreme events. We use the following family of Gabor basis elements consisting of

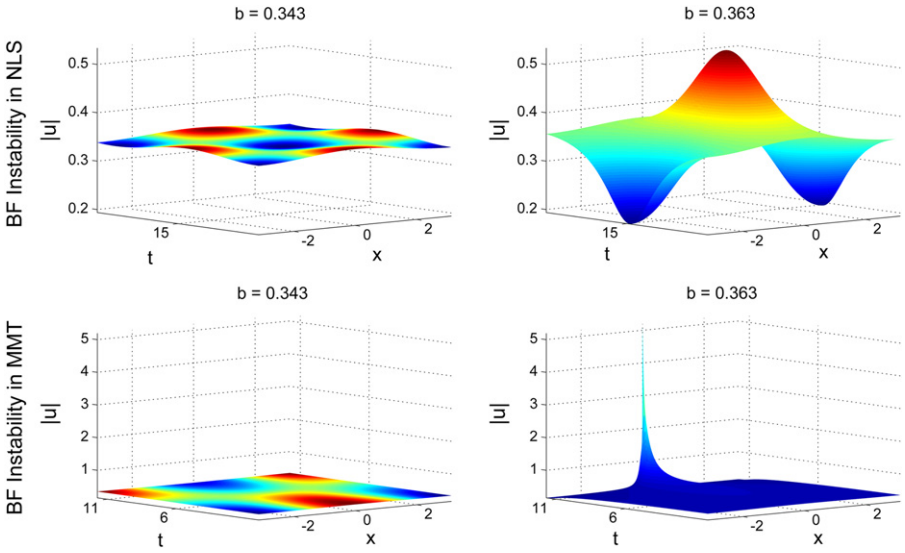

Fig. 5. Benjamin–Feir instability for the NLS equation (top) and the MMT model (bottom) with ($\alpha = 0.5$, $\beta = 0$, $\lambda = -4$).

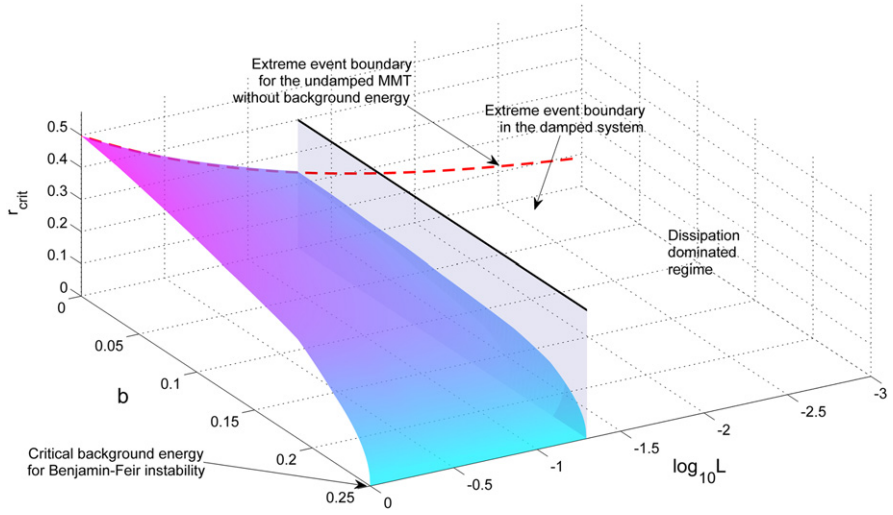

Fig. 6. Numerically computed critical energy norm of localized perturbations that lead to extreme events in the presence of background energy for the damped MMT model ($\alpha = 0.5$, $\beta = 0$).

complex exponentials multiplied by Gaussian window functions:

$$v_n(x; x_c) \triangleq \exp\left[-2\frac{d(x, x_c)^2}{L^2}\right] e^{i2\pi nx/L}, \quad n = 0, 1, 2, \ldots \tag{5}$$

where $d(x, x_c) = \min(|x - x_c|, 2\pi - |x - x_c|)$ expresses the distance from the center point x_c measured in the periodic domain. We then compute the Gabor projection coefficients of the solution.

$$Y_n(x_c, t) \triangleq \langle u(x, t), v_n(x; x_c)\rangle / \|v_n(x; x_c)\|^2,$$

where $\langle \cdot, \cdot \rangle$ denotes the standard L^2 inner product. We noted in Section 3 that there is a critical scale $L_c \approx 0.01$ that is most sensitive to the formation of an extreme event, in that the required energy to trigger an extreme event is smallest at this particular scale. In practice, we have observed that these extreme events typically originate by energy localization in a slightly larger scale than L_c. This motivates our choice of $L = \pi/100 \approx 3L_c$, which is still extremely sensitive to small perturbations (Fig. 4). After a sufficient amount of energy is localized in this scale, an extreme peak is then produced as energy is transferred into the smaller scales until it reaches the scale at which selective dissipation is present. We have chosen $L = 0.031$ based on this argument with the goal of using the coefficient Y_0 as an indicator of an upcoming extreme event.

In Fig. 7 we present the Gabor coefficients in space and time during the occurrence of a pair of extreme events. More specifically, in the first row (left) we display the envelope $|u|$ during the formation of a pair of extreme waves in the (x, t) space. In the second row, we show the Gabor basis elements v_n and in the third row we show the modulus of the Gabor coefficients, $|Y_n|$. In the top-right panel we display the Euclidean sum of the oscillatory Gabor coefficients, $E_h = \sum_{n\geq 1} \|Y_n\|^2$, which expresses the energy that 'lives' in high wavenumbers.

For the Gabor coefficients that correspond to the oscillatory basis elements $(Y_1, Y_2, Y_3, \ldots)$, we note that away from the region of the extreme events, wave components propagate almost independently, according to the dispersion relation, in a close to linear fashion. The energy of the non-oscillatory mode (expressed through the Gabor coefficient Y_0) presents a more static (non-propagating) behavior with high intensity that builds up before the extreme event. During the strongly non-linear phase (of the extreme response), the Gabor coefficients of the oscillatory basis elements are not governed by the dispersion relation anymore, but they also present a more static (non-propagating) behavior characterized by a large build up of their energy. This is the result of a strong, nonlinear energy transfer initiated from the unstable lengthscale L, described

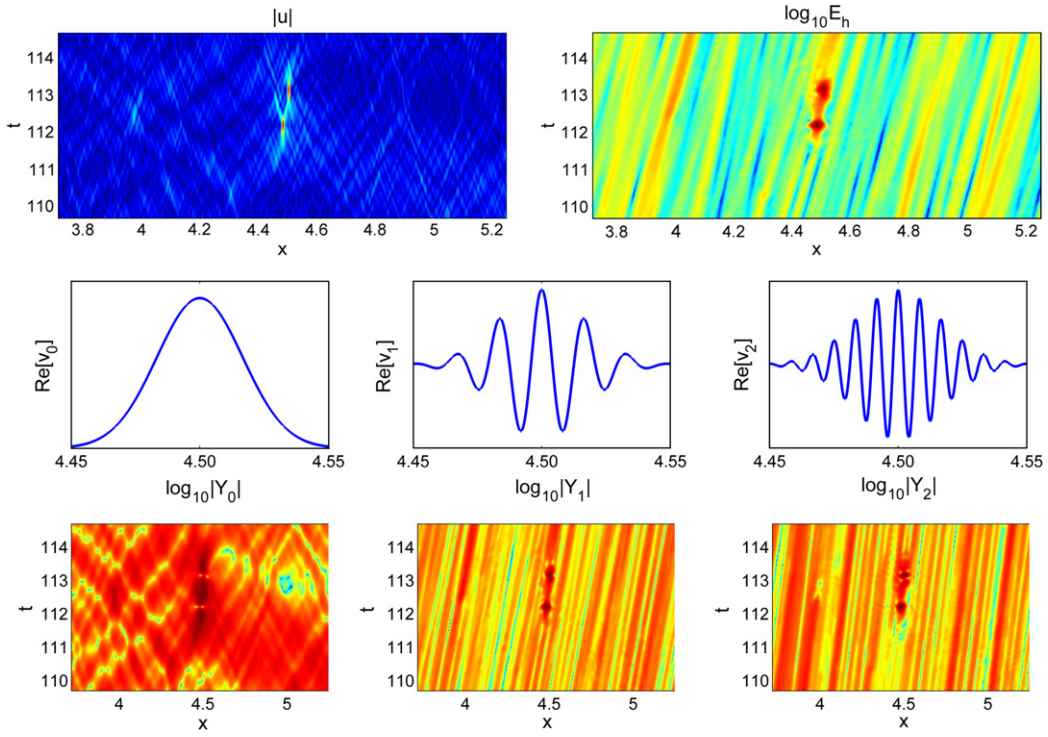

Fig. 7. Energy transfer during an extreme event. Top row: extreme event shown in (x, t) space together with the high wavenumber energy $E_h = \sum_{n\geq 1} \|Y_n\|^2$. Second row: Gabor basis elements $v_n(x; 0)$. Third row: modulus of the Gabor coefficients $\|Y_n(x_c, t)\|$.

by the non-oscillatory mode v_0, and ending to higher wavenumbers where it is dissipated (Figs. 7 and 8).

Statistics and energy transfers during the dissipation phase. The strong nonlinear energy transfer from the unstable scale L to smaller scales is manifested by the non-Gaussian statistics of the Gabor coefficients during an extreme event. The connection between nonlinear energy transfers and non-Gaussian statistics has been rigorously established in [12,13,35] in the context of viscous turbulent flows. Consider an orthonormal set of modes v_i, $i = 0, 1, 2, \ldots, n_c$ (although the modes (5) are not orthonormal, they are nearly so) which are active during the occurrence of an extreme event and let the background stage (i.e. the full stochastic solution during a non-extreme regime) described by $u(x, t)$. Then, the MMT equation with $\alpha = 0.5$, $\beta = 0$

$$u_t = -i\,|\partial_x|^{1/2}\,u - i\lambda\,|u|^2\,u + Du$$

will take the projected form for each v_i

$$\frac{dY_i}{dt} = \left\langle \left[D - i\,|\partial_x|^{1/2}\right] u,\, v_i \right\rangle + \sum_k Y_k \left\langle \left[D + |\partial_x|^{1/2}\right] v_k,\, v_i \right\rangle$$

$$- i\lambda \left\langle \left| u + \sum_k Y_k v_k \right|^2 \left(u + \sum_k Y_k v_k \right),\, v_i \right\rangle. \tag{6}$$

The growth rate of the energy of Y_i will have the form

$$\frac{d\,|Y_i|^2}{dt} = \frac{dY_i}{dt} Y_i^* + \frac{dY_i^*}{dt} Y_i = 2\mathrm{Re}\left[\frac{dY_i}{dt} Y_i^*\right].$$

Note that in Eq. (6) the first line on the right hand side involves either energy conserving terms such as wave dispersion or negative definite terms such as dissipation (which occurs for high wavenumbers only). All the other contributions towards changes of $|Y_i|^2$ will only occur through the nonlinear interactions of the modes:

$$\left.\frac{d\overline{|Y_i|^2}}{dt}\right|_{NL} = -2\mathrm{Re}\left[\overline{i\lambda \left\langle \left| u + \sum_k Y_k v_k \right|^2 \left(u + \sum_k Y_k v_k \right),\, v_i \right\rangle Y_i^*}\right]$$

where the bar denotes ensemble average. We focus on the energy transfer regime from the mode v_0 to higher wavenumber modes during an extreme event.

We compute the Gabor coefficients for 400 values of x_c equally distributed between 0 and 2π, with $L \approx 3L_c$. We then classify each point (x_c, t) into two regimes: points nearby an extreme event and points away from extreme events. For each of these groups, we compute the joint statistics of the Gabor coefficients using data from an ensemble of MMT simulations with random initial data (details of these simulations are given in Section 2.1). Fig. 9 displays the joint statistics of the imaginary parts of Y_0, Y_1, and Y_2 near (left subplot) and far (right subplot) from extreme events.

Away from extreme events the isosurfaces of the probability density function are elliptical, indicating that the Gabor coefficients are nearly Gaussian in this regime. Moreover, the time oscillatory character of the wave components results in zero average value (in the ensemble sense) for all the corresponding Gabor coefficients $\overline{Y_i} = 0$, $i = 1, 2, \ldots$ (for both regimes). Due to this fact, as well as the Gaussian distribution of the coefficients Y_i in the non-extreme events regime, the average change of their energy due to nonlinear interactions becomes zero.

On the other hand, the statistics near extreme events are highly non-Gaussian, with Y_0 exhibiting a bimodal distribution. The real parts of the Gabor coefficients are distributed similarly. This non-Gaussian distribution is directly related to the energy cascade from the non-oscillatory mode to the strongly dissipative, high wavenumber modes.

Dynamics during the built-up phase of the extreme event. In Fig. 10, we show how an extreme event trajectory emerges out of the Gaussian background describing the heat bath of waves propagating under the dominant effect of the dispersion relation. From the same figure it is clearly illustrated how extreme events are associated with large values of $|Y_0|$. The nature of this association is particularly interesting: $|Y_0|$ becomes large just *before* (and after) extreme events. An example of this behavior is displayed in Fig. 11, where we observe the increase of $|Y_0|$ while the overall response

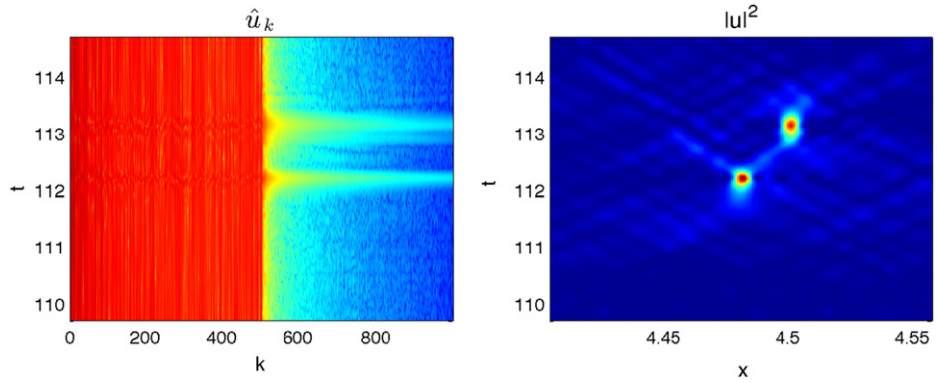

Fig. 8. Energy transfer to higher wavenumbers during the occurrence of extreme events shown in terms of the moduli of the Fourier coefficients for the MMT model.

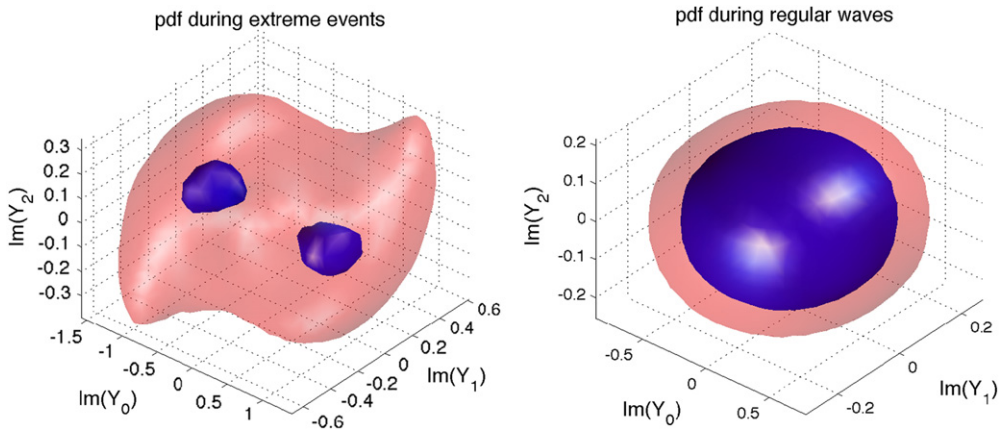

Fig. 9. Isosurfaces of the joint pdf of the imaginary parts of Y_0, Y_1, and Y_2 near to (left) and away from (right) extreme events.

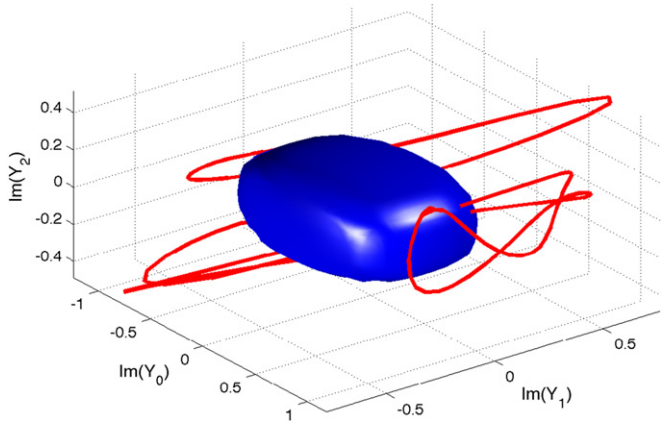

Fig. 10. The red curves show trajectories of the imaginary parts of Y_0, Y_1, and Y_2 during extreme events. The blue surface is an isosurface of the joint density function for the imaginary parts of Y_0, Y_1, and Y_2 containing 97% of the total probability—this shape is dominated by the Gaussian random waves that propagate with random phase under the effect of dispersion and weak nonlinearity. (For interpretation of the references to color in this figure legend, the reader is referred to the web version of this article.)

field $|u|$ has regular values. This growth continues until we have an extreme event and it is followed by a sudden drop that is associated with an energy transfer to high wavenumbers illustrated by the energy E_h (as described previously). This agrees with observations by Cai et al. [18] that these extreme events form by focusing energy to high wavenumbers until saturation at a critical scale, at which point they radiate energy back to larger scales. We are particularly interested in the predictive utility of the localized energy $|Y_0|$ buildup that occurs before extreme events, often 1–2 time units in advance for the considered set of parameters.

This phenomenon agrees with our analysis from Section 3, where we showed that a sufficient amount of localized energy is sufficient to trigger an extreme event. These localizations of energy occur randomly through the dispersive propagation of waves that have random phases. Due to the localized nature of v_0, the associated Gabor coefficient $|Y_0|$ measures such localized energy and is thus an indicator of an extreme event in the near future. When the extreme event occurs, energy is transferred into the more oscillatory modes (v_1, v_2, ...), but the Gabor coefficients associated with these modes lack predictive utility since they grow simultaneously with, rather than prior to, the extreme event (see Fig. 11).

5. Short-term prediction of extreme events

The Gabor coefficient Y_0 is a measure of energy localized at a particularly sensitive lengthscale, at which only a small amount of energy is necessary to trigger an extreme event. Thus, large values of $|Y_0|$ imply that it is highly likely that (1) an extreme event will occur in the near future or (2) an extreme event has occurred in the recent past (see Fig. 11). We now use this fact to develop short-term predictive capacity for extreme events. To do so, we first compute, for various values of $\mathcal{Y}_0$, the following family of probability distributions:

$$F_{\mathcal{Y}_0}(\mathcal{U}) \triangleq \mathcal{P}\left(\max_{\substack{|x^*-x_c|<L \\ t^*\in[t-1.5,t+1.5]}} |u(x^*,t^*)| > \mathcal{U} \mid |Y_0(x_c,t)| = \mathcal{Y}_0 \right). \quad (7)$$

That is, given a particular value of $|Y_0(x_c,t)|$, we compute the probability that $|u|$ exceeds $\mathcal{U}$ nearby. The timescale of 1.5 time units has been chosen based on our observation of the time required for the transition from large values of $|Y_0|$ to extreme values of $|u|$. We

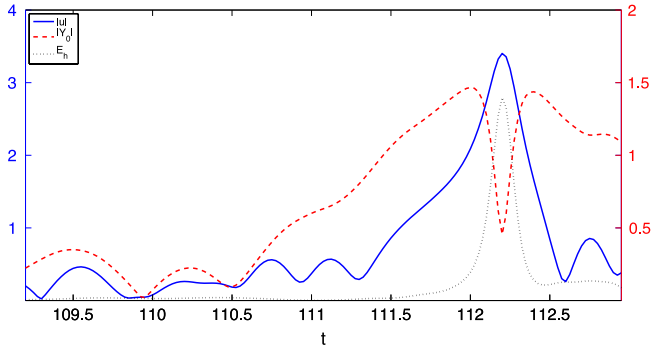

Fig. 11. Time evolution of $|u|$, $|Y_0|$, and E_h at a spatial location of an extreme event. The y-axis scale on the left corresponds to $|u|$; the right y-axis scale corresponds to $|Y_0|$ and E_h.

compute these distributions from an ensemble of 300 simulations, each spanning 100 time units (see Section 2.1 for simulation details).

In Fig. 12, we display the family of conditional density functions corresponding to (7). Clearly there is a critical value of $|Y_0|$ which, when exceeded, implies that a nearby extreme event is highly likely. We stress that even though we compute the conditional statistics of $u(x^*, t^*)$ given $|Y_0(x, t)|$ for $t^* \in [t-1.5, t+1.5]$, the large values of $|Y_0|$ above the bifurcation point in Fig. 12 do not occur *during* the extreme event itself. These large $|Y_0|$ occur before and after the extreme event-during the extreme event itself $|Y_0|$ is not large (Fig. 11). As discussed below, the large values of $|Y_0|$ can be discarded, since in our observation of many simulations large $|Y_0|$ that occur *after* extreme events do not initiate energy transfers to smaller scales. In some ways this is similar to the demodulation phase of breather type solutions to nonlinear Schrödinger initiated by the Benjamin–Feir instability [34,32]. Although a precise mathematical explanation of this phenomena would be meaningful, for the purposes of this work the simple ad-hoc criteria (ignoring $|Y_0|$ that occur just after extreme events) is effective. As we discuss below, we obtain a predictive scheme with a false negative rate of less than 1%.

It is straightforward to connect the bifurcation in the distributions displayed in Fig. 12 to our theoretical analysis from Section 3. When $|Y_0| > 1.1$, the likelihood of a nearby extreme event increases dramatically. We may use the definition of v_0 to compute the energy level at which this bifurcation occurs at the critical lengthscale $L = 0.031$:

$$1.1\|v_0\| = 1.1\sqrt{\int e^{-2(x/L)^2}\,dx} = 1.1\sqrt{L}\sqrt[4]{\pi/2} \approx 0.22.$$

This critical energy value of 0.22 agrees well with our results from Section 3, where we found that Gaussian initial data localized at lengthscale $L = 0.031$ initiated extreme events if the energy level exceeds approximately 0.2 (see Fig. 4). These results from Section 3 were performed for localized states with a zero background, but the agreement of this analysis with the bifurcation energy level in Fig. 12 is significant. Specifically, it suggests that the same localized energy instability discussed in Section 3 for toy examples triggers the formation of extreme events out of more complex states.

We now compute the probability of a nearby extreme event, given a particular value of $|Y_0|$. Here we define an extreme event as an instance where $|u| > 2.5$. This value is greater than twice the significant wave height-here taken to be four times the typical deviation of the wave field (and is consistent with the informal definition of rogue waves in the ocean [1]). This probability, displayed in the right half of Fig. 12, is simply $F_{y_0}(2.5)$ from (7).

We now analyze the performance of the computed extreme event probability data from Fig. 12 as a predictive scheme. At a given time, we compute $|Y_0(x_c, t)|$ for various values of x_c and use our compiled statistics (Fig. 12) to estimate the probability of an extreme event. If this probability exceeds 0.8, we predict that an extreme event will occur. Choosing a larger probability threshold value would decrease our rate of false positives; choosing a smaller value would increase this rate, but would have the benefit of increasing the amount of time by which extreme events are predicted in advance. We found that a probability threshold of 0.8 provides a reasonable balance between these two effects (false positive rate versus advanced warning time). Essentially the predictive scheme measures the probability that a given combination of phases between wave components (the current form of the wave field) belongs to the domain of attraction of an extreme wave.

We tested this scheme on 50 simulations of (1). These simulations were *not* used to compute the statistics in (7) and Fig. 12. In these simulations, we predicted an extreme event 191 times, and 155 correctly predicted an extreme event, meaning that the false positive rate was only 18.9%. There was only 1 extreme event that was not predicted by our scheme, which means that the false negative rate was less than 1%. As mentioned in Section 4, in addition to preceding extreme events, large values of Y_0 can occur after extreme events as energy is being transferred to larger scales. However, large values of $|Y_0|$ in this particular situation do not actually imply that an extreme event is forthcoming. To avoid false positive predictions that such behavior would generate, we "turn off" our predictive scheme in the spatial region nearby the extreme event for the following 1 time unit. Since our false negative rate is less than 1%, ignoring these large values of $|Y_0|$ immediately following an extreme event does not meaningfully degrade the accuracy of our predictive scheme.

In Fig. 13 we present the spatial distribution of the probabilistic predictor (left) and the actual wave field (right) for one random realization. As we observe the computed criterion captures accurately not only the temporal but also the spatial position of the extreme wave. The same conclusions can be drawn from Fig. 14 where our prediction scheme is often able to predict extreme events a full 1–2 time units in advance.

6. Discussion and conclusions

We have examined the synergistic activity of nonlinearity, dispersion, and dissipation towards the formation of extreme events in a one-dimensional prototype system that possesses four-wave resonant interactions, the focusing MMT equation. The latter provides a relatively simple model of extreme events arising out of a nearly Gaussian background with broad-band spectrum, mimicking in this way many features of rogue waves in the ocean. Through analytical and numerical tools we have shown that the MMT is highly sensitive to *localized* perturbations of a particular critical lengthscale (Fig. 4), which we analyze thoroughly. We show the existence of a family of solutions with a scale-invariance property and based on this fact we quantify the required localized amount of energy that triggers an extreme event. Although the existence of a critical energy level for extreme events is certainly related to the modulation instability, our analysis illustrates that even zero-background-energy states can lead to an extreme event if a localized perturbation of appropriate lengthscale and intensity is applied. These localized perturbations can occur randomly through the dispersive propagation of waves with random relative phase.

We have illustrated that these extreme events are characterized by low-dimensionality and we have use a spatially localized basis, a Gabor basis to describe their characteristics. By performing a statistical analysis of the Gabor coefficients we have been able to develop an inexpensive predictive scheme that is reliable with few false positives and false negatives. Furthermore, our scheme shows a high degree of spatial skill and issues warnings in advance (often

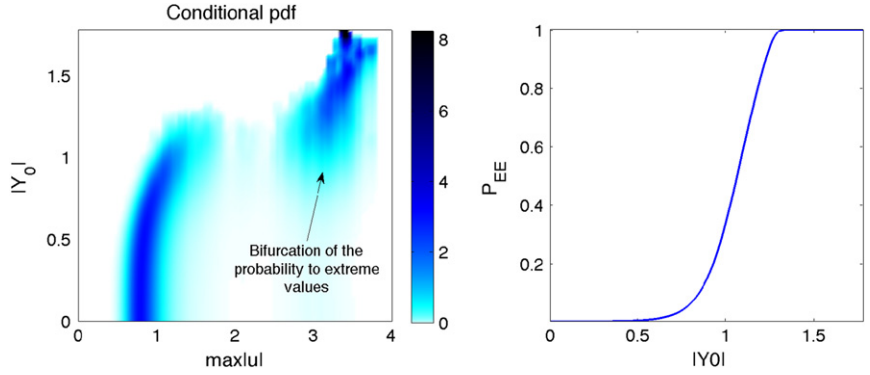

Fig. 12. Left: family of conditional densities of maximum nearby $|u|$ given a current value of $|Y_0|$. Right: probability of an extreme event in nearby given $|Y_0|$.

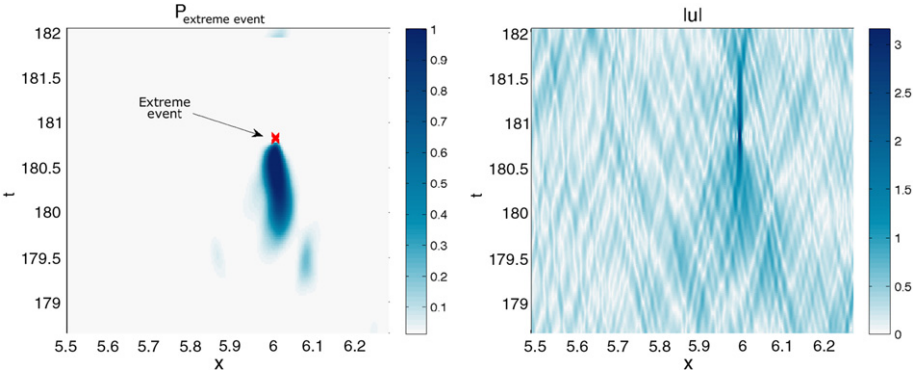

Fig. 13. Left: spatial distribution of probability for a nearby extreme event. Right: $|u|$ as a function of space and time. The above figure shows the spatial skill of our predictive scheme.

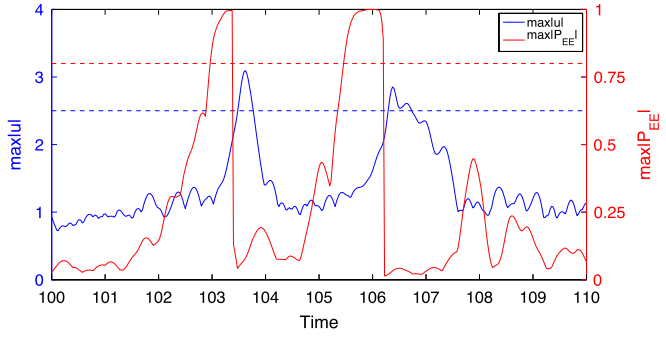

Fig. 14. Spatial maximum values of $|u|$ and extreme event probability, showing that our predictive scheme is able to give advance warning of extreme events.

1–2 time units before the extreme event). Future research efforts include the extension of the prediction window by combining the presented approach with nonlinear filtering techniques [36]. We are also interested on applying the presented framework in more realistic two dimensional nonlinear wave models and a current research effort is focused on the wave equation by Trulsen et al. [37] which, like the MMT model, includes the exact dispersion relation for gravity waves over deep water.

Acknowledgments

This research effort is funded by the Naval Engineering Education Center through Grant 3002883706. We are grateful to Dr. Craig Merrill (technical point of contact for this project) for numerous motivating discussions and support. We would like to thank Prof. Andrew Majda who suggested the MMT model as a prototype system for extreme events as well as for numerous other stimulating comments. We are grateful to Dr. Ian Grooms for providing a version of his numerical solver for the MMT system, as well as to Lake Bookman for helpful discussions.

References

[1] K. Dysthe, H. Krogstad, P. Muller, Oceanic rogue waves, Annu. Rev. Fluid Mech. 40 (2008) 287.
[2] N. Akhmediev, E. Pelinivsky, Editorial – introductory remarks on 'discussion and debate: Rogue waves – towards a unifying concept?', Eur. Phys. J. Spec. Top. 185 (2010) 1–4.
[3] P. Muller, C. Garrett, A. Osborne, Rogue waves, Oceanography 18 (3) (2005) 66–75.
[4] W. Xiao, Y. Liu, G. Wu, D. Yue, Rogue wave occurrence and dynamics by direct simulations of nonlinear wave-field evolution, J. Fluid Mech. 720 (2013) 357–392.
[5] J. Neelin, B. Lintner, B. Tian, Q. Li, L. Zhang, P. Patra, M. Chahine, S. Stechmann, Long tails in deep columns of natural and anthropogenic tropospheric tracers, Geophys. Res. Lett. 37 (2010) L05804.
[6] A.J. Majda, B. Gershgorin, Quantifying uncertainty in climate change science through empirical information theory, Proc. Natl. Acad. Sci. 107 (2010) 14958–14963.
[7] V. Kishore, M. Santhanam, R. Amritkar, Extreme events and event size fluctuations in biased random walks on networks, Phys. Rev. E 85 (2012) 056120.
[8] P. Pourbeik, P. Kundur, C. Taylor, The anatomy of a power grid blackout—root causes and dynamics of recent major blackouts, IEEE Power Energy Mag. 4 (5) (2006) 22–29.
[9] E. Kreuzer, W. Sichermann, The effect of sea irregularities on ship rolling, Comput. Sci. Eng. 8 (2006) 26–34.
[10] P. Janssen, Nonlinear four-wave interactions and freak waves, J. Phys. Oceanogr. 33 (2003) 863–884.
[11] M. Onorato, A. Osborne, M. Serio, L. Cavaleri, C. Brandini, C. Stansberg, Extreme waves, modulatinoal instability and second order theory: wave flume experiments on irregular waves, Eur. J. Mech. B/Fluids 25 (2006) 586–601.
[12] T.P. Sapsis, Attractor local dimensionality, nonlinear energy transfers, and finite-time instabilities in unstable dynamical systems with applications to 2D fluid flows, Proc. R. Soc. A 469 (2153) (2013) 20120550.
[13] T.P. Sapsis, A.J. Majda, A statistically accurate modified quasilinear Gaussian closure for uncertainty quantification in turbulent dynamical systems, Physica D 252 (2013) 34–45.
[14] A. Osborne, The random and deterministic dynamics of 'rogue waves' in unidirectional, deep-water wave trains, Mar. Struct. 14 (2001) 275–293.
[15] A.J. Majda, M. Branicki, Lessons in uncertainty quantification for turbulent dynamical systems, Discrete Contin. Dyn. Syst. 32 (2012) 3133–3221.
[16] A. Majda, D.W. McLaughlin, E. Tabak, A one-dimensional model for dispersive wave turbulence, J. Nonlinear Sci. 6 (1997) 9–44.
[17] D. Cai, A.J. Majda, D.W. McLaughlin, E.G. Tabak, Spectral bifurcations in dispersive wave turbulence, Proc. Natl. Acad. Sci. 96 (25) (1999) 14216–14221.

[18] D. Cai, A. Majda, D. McLaughlin, E.G. Tabak, Dispersive wave turbulence in one dimension, Physica D 152–153 (2001) 551–572.
[19] V. Zakharov, P. Guyenne, A. Pushkarev, F. Dias, Wave turbulence in one-dimensional models, Physica D 152–153 (2001) 573–619.
[20] V. Zakharov, F. Dias, A. Pushkarev, One-dimensional wave turbulence, Phys. Rep. 398 (2004) 1–65.
[21] A. Pushkarev, V. Zakharov, Quasibreathers in the MMT model, Physica D 248 (2013) 55–61.
[22] I. Grooms, A.J. Majda, Stochastic superparameterization in a one-dimensional model for wave turbulence, Commun. Math. Sci. 12 (3) (2014) 509–525.
[23] G.J. Komen, L. Cavaleri, M. Donelan, K. Hasselmann, S. Hasselmann, P. Janssen, Dynamics and Modeling of Ocean Waves, Cambridge University Press, 1994.
[24] M. Onorato, A. Osborne, S. Bertone, Freak waves in random oceanic sea states, Phys. Rev. Lett. 86 (25) (2001) 5831–5834.
[25] Y. Chung, P. Lushnikov, Strong collapse turbulence in a quintic nonlinear Schrödinger equation, Phys. Rev. E 84 (2011).
[26] S. Cox, P. Matthews, Exponential time differencing for stiff systems, J. Comput. Phys. 176 (2) (2002) 430–455.
[27] A.-K. Kassam, L.N. Trefethen, Fourth-order time-stepping for stiff PDEs, SIAM J. Sci. Comput. 26 (4) (2005) 1214–1233.
[28] H. Berland, B. Skaflestad, W.M. Wright, Expint—a matlab package for exponential integrators, ACM Trans. Math. Softw. (TOMS) 33 (1) (2007) 4.
[29] T.B. Benjamin, J.E. Feir, The disintegration of wave trains on deep water, J. Fluid Mech. 27 (1967) 417–430.
[30] T.B. Benjamin, Instability of periodic wavetrains in nonlinear dispersive systems, Proc. R. Soc. Lond. Ser. A Math. Phys. Eng. Sci. 299 (1456) (1967) 59–76.
[31] V. Zakharov, Stability of periodic waves of finite amplitude on the surface of a deep fluid, J. Appl. Mech. Tech. Phys. 9 (2) (1968) 190–194.
[32] H.C. Yuen, W.E. Fergusen, Relationship between Benjamin–Feir instability and recurrence in the nonlinear Schrodinger equation, Phys. Fluids 21 (8) (1978).
[33] B. Rumpf, A. Newell, Wave instability under short-wave amplitude modulations, Phys. Lett. A 377 (2013) 1260–1263.
[34] M.J. Ablowitz, B. Herbst, On homoclinic structure and numerically induced chaos for the nonlinear Schrodinger equation, SIAM J. Appl. Math. 50 (2) (1990) 339–351.
[35] T.P. Sapsis, A.J. Majda, Statistically accurate low order models for uncertainty quantification in turbulent statistically accurate low order models for uncertainty quantification in turbulent dynamical systems, Proc. Natl. Acad. Sci. 110 (2013) 13705–13710.
[36] A.J. Majda, J. Harlim, Filtering Complex Turbulent Systems, Cambridge University Press, 2012.
[37] K. Trulsen, I. Kliakhandler, K. Dysthe, M. Velarde, On weakly nonlinear modulation of waves on deep water, Phys. Fluids 12 (2000) 2432.